IN-39-CR
10371
P 34

FAILURE PREDICTION OF THIN BERYLLIUM SHEETS USED IN SPACECRAFT STRUCTURES

SEMIANNUAL STATUS REPORT

Period: July 1, 1990, to December 31, 1990

Principal Investigator: Dr. Paul N. Roschke
Research Assistants: Photios Papados, Edward Mascorro

Texas A&M University
Department of Civil Engineering
College Station, Texas 77843-3136

NASA Grant Number: NAG 9-280

FAILURE PREDICTION OF THIN BERYLLIUM SHEETS USED IN SPACECRAFT STRUCTURES

Introduction

In an attempt to predict failure for cross-rolled beryllium sheet structures higher order macroscopic failure criteria are used. These require the knowledge of in-plane uniaxial, biaxial, and shear strengths. The current report includes test results for in-plane biaxial tension, uniaxial compression for two different material orientations, and shear. All beryllium specimens have the same chemical composition (see Table 1). In addition, all experimental work was carried out in a controlled laboratory environment. Numerical simulation complements these tests. A brief bibliography supplements references listed in a previous report.

TABLE *1. Chemical Composition of Beryllium Specimens*

Element	Chemical Composition (weight %)
Be	99.10
BeO	1.00
Fe	0.06
C	0.12
Al	0.03
Mg	-0.01
Si	0.02

Biaxial State of Stress

Experimental Studies

A biaxial state of stress using a uniaxially loaded specimen was achieved by orienting the material axes 45° from the direction of the load (Fig. 1). To minimize the possibility of failure at the grips, a total of three specimens were designed with curved transitions; also, aluminum pads were epoxied to the ends (Fig. 2). In-plane strain was measured using bonded Micro-Measurement precision strain gages (Types CEA-06-062UR-350 and WK-06-062AP-350). Rosette gages were placed on both sides of each specimen and a single free-field gage was placed on one side of

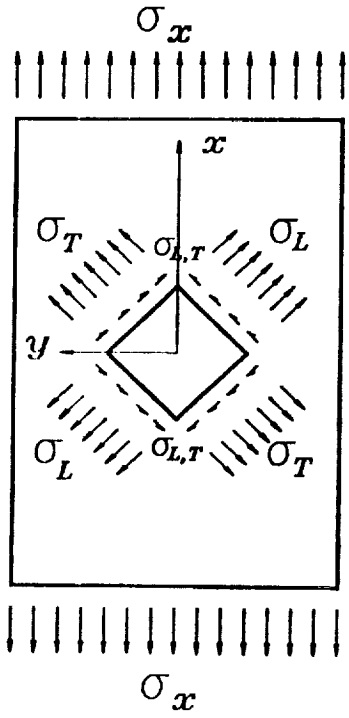

Figure *1 Stress Block Diagram*

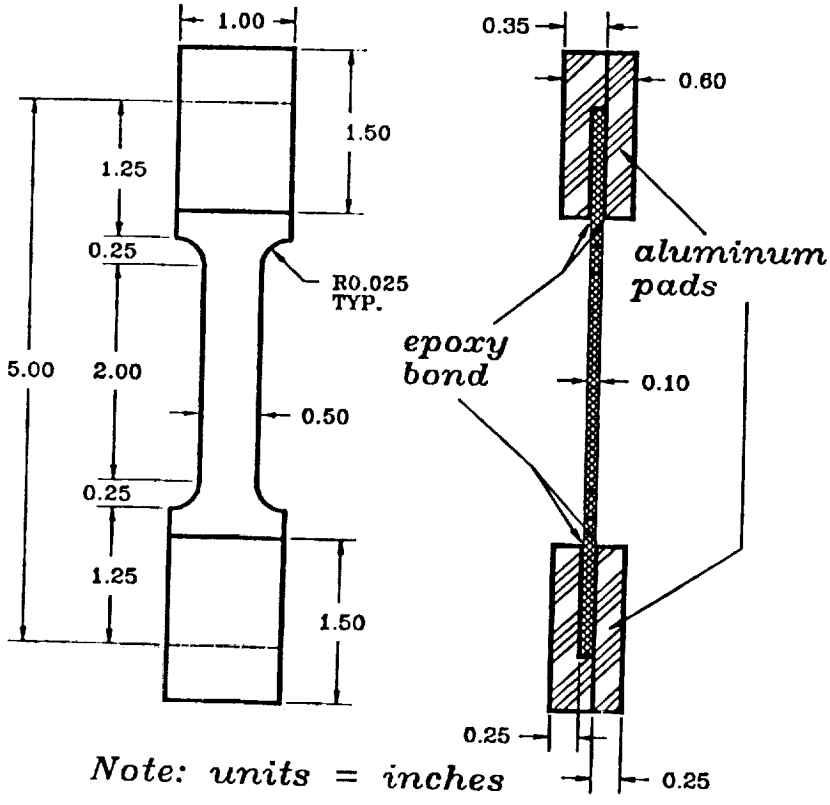

Figure *2 Specimen Configuration*

each specimen for measurement of strain normal to the direction of the applied load (Fig. 3). A Material Testing System (MTS) Extensometer (Model 632.86B-03) was used to record through-thickness strains. Each specimen was loaded using an 89-kN (20-kip) capacity MTS uniaxial testing machine.

Test Results

Stress-strain curves are plotted for each gage (see Figs. 4-6 for typical examples). An average Young's modulus is measured to be 29.5×10^4 MPa (42.8×10^6 psi). Poisson's ratio for in-plane and through-thickness deformations is 0.096 and 0.14, respectively. These ratios are calculated as follows:

$$\nu_{y,x} = E_x/S_{y,x} \quad (1)$$

$$\nu_{z,x} = E_x/S_{z,x} \quad (2)$$

where E_x is the conventional Young's Modulus for the loaded "x" direction, and $S_{y,x}$ (or $S_{z,x}$) is the measured stiffness in the "y" (or "z") direction due to stress in the loaded "x" direction (see Fig. 1 for directions). Failure stresses for each specimen are listed in Table 2.

TABLE 2. *Failure Stress of Each Specimen*

Specimen Number		Failure Stress MPa	(ksi)
1		397.55	(57.66)
2		529.24	(76.76)
3		536.96	(77.88)
	Average*	533.10	(77.32)

*Computed using Specimens 2 and 3 only.

As indicated in Table 2, Specimen 1 failed at a very low load, which occurred almost immediately after yield. This may have been caused by the MTS clip gage scratching the surface or from a flaw in the specimen. To avoid scratching the surface 0.2032-mm (0.008-in.) thick brass shims were placed between specimen 2 and the MTS clip gage's contact points. Brass shims were not placed on specimen 3 because it was loaded to failure chronologically before the other two specimens.

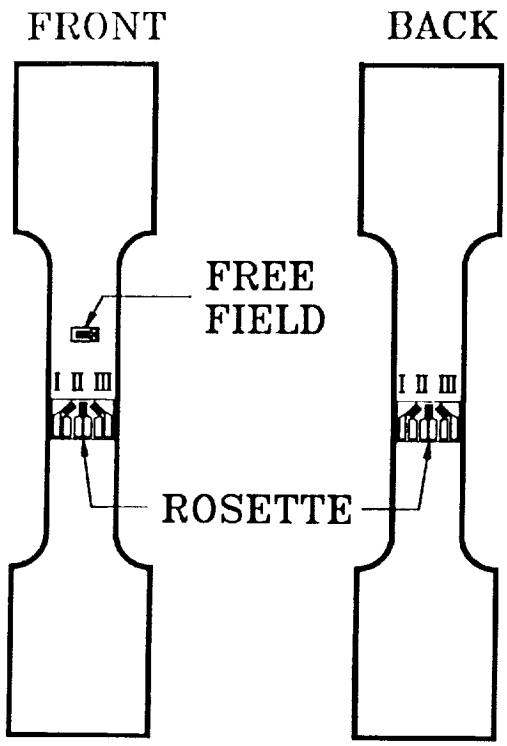

Figure *3 Strain Gage Location*

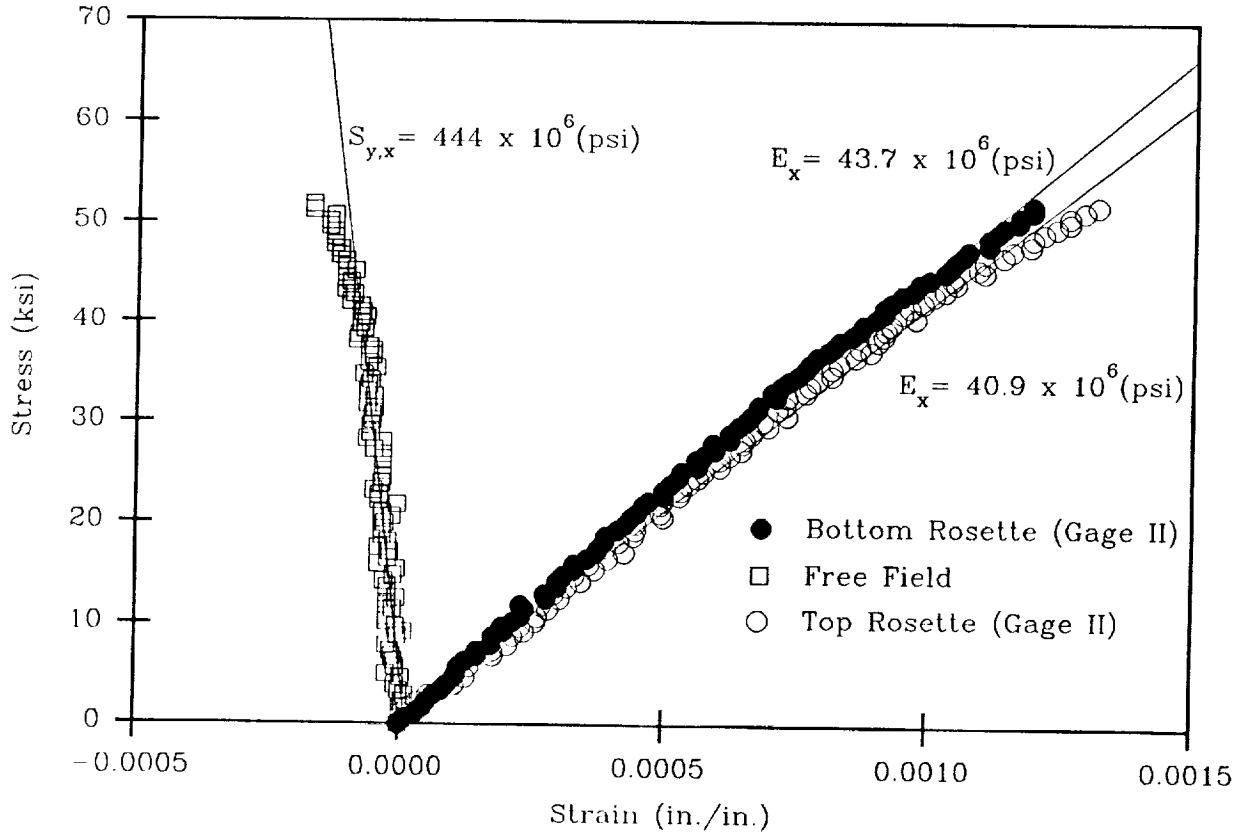

Figure *4 Stress vs. Strain in x and y Directions for Specimen 2*

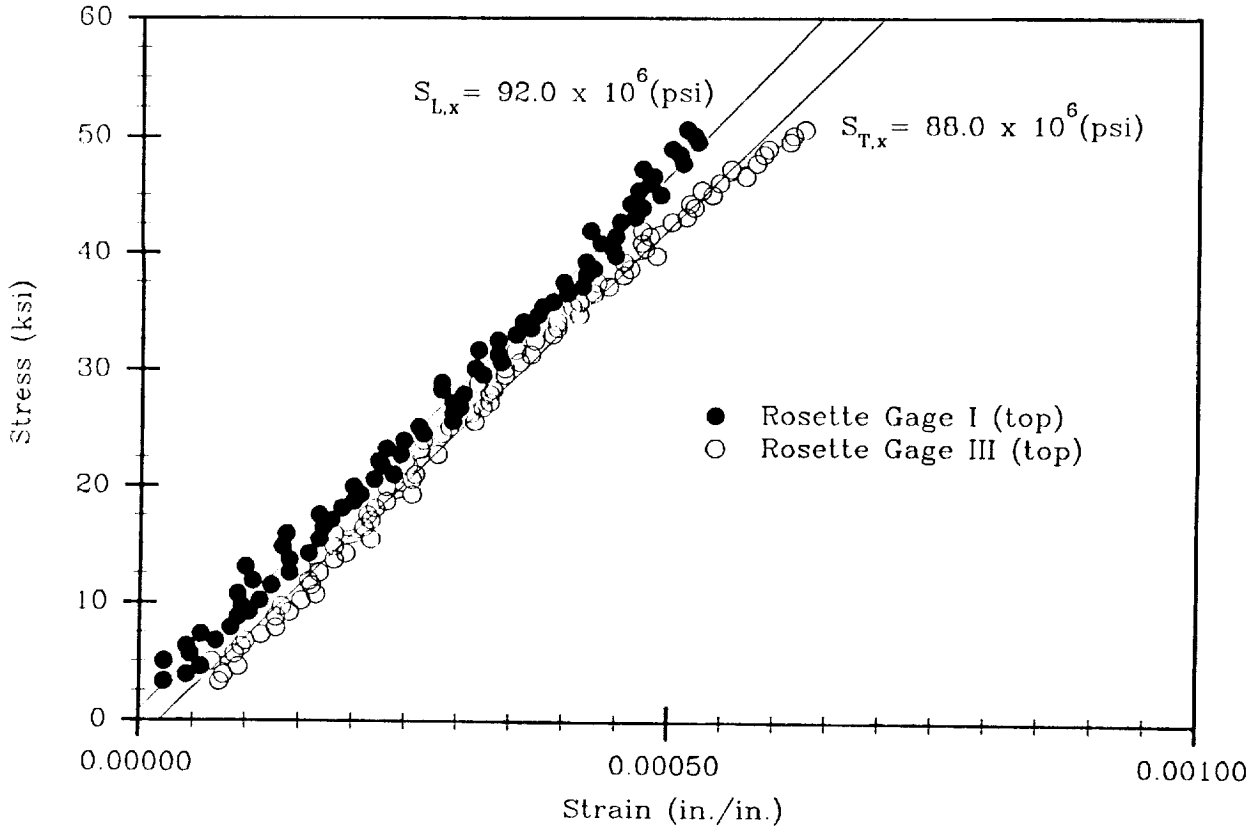

Figure *5 Stress vs. Strain in Long and Transverse Material Directions for Specimen 2*

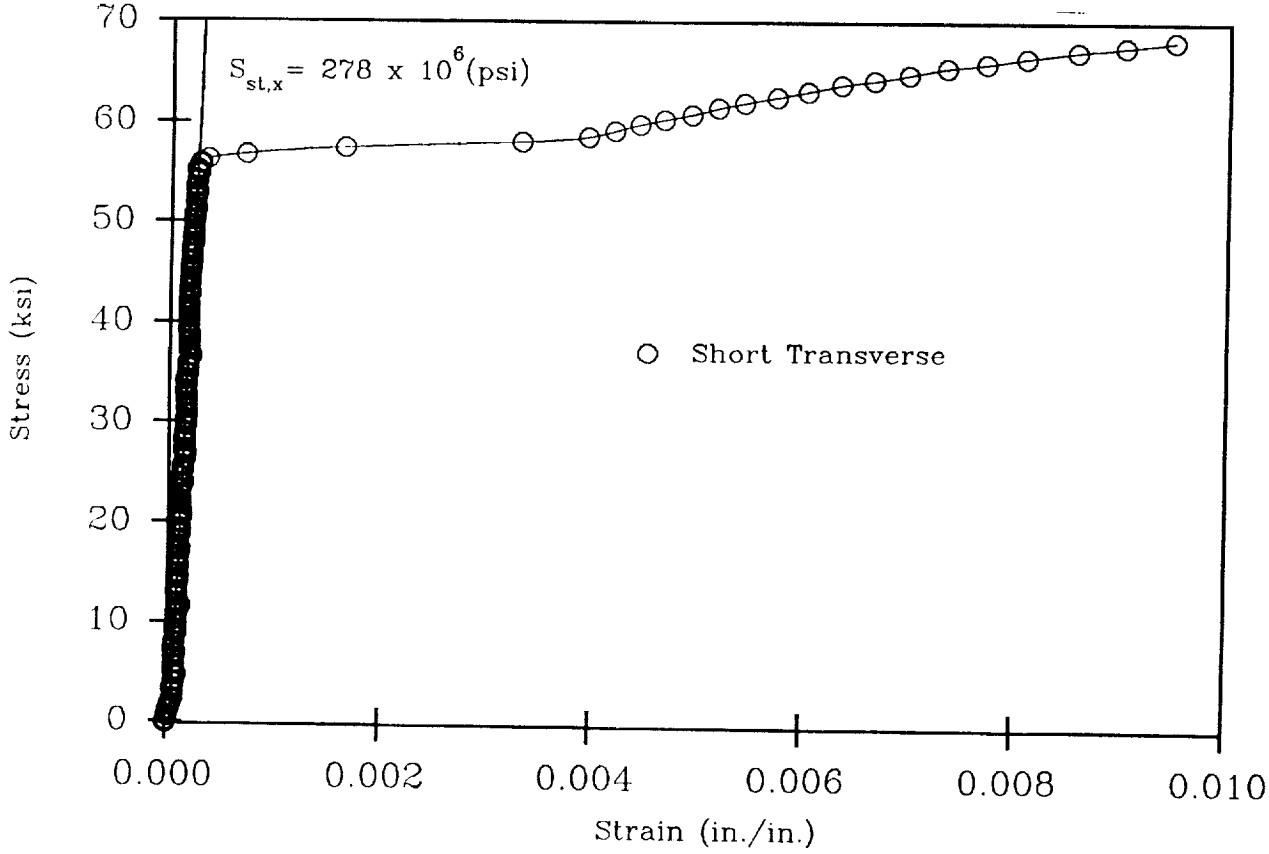

Figure *6 Stress vs. Strain in Short Transverse Material Directions for Specimen 2*

Elastic Studies

In order to compare elastic properties from an earlier test [1] with data obtained from this experiment, the stress tensor aligned with the loaded axis is transformed to the material axis [2]. (Note that all calculations are shown in Appendix (A)). Components of the transformed stress tensor are then substituted into the following three-dimensional orthotropic elasticity equations that relate stress and strain [1]:

$$\epsilon_L = (\sigma_L/E_L) - \nu_{L,T}(\sigma_T/E_T) - \nu_{L,ST}(\sigma_{ST}/E_{ST}) \quad (3)$$

$$\epsilon_T = (\sigma_T/E_T) - \nu_{T,L}(\sigma_L/E_L) - \nu_{T,ST}(\sigma_{ST}/E_{ST}) \quad (4)$$

$$\epsilon_{ST} = (\sigma_{ST}/E_{ST}) - \nu_{ST,L}(\sigma_L/E_L) - \nu_{ST,T}(\sigma_T/E_T) \quad (5)$$

$$\gamma_{L,T} = \tau_{L,T}/G_{L,T} \quad (6)$$

Manipulation of Eqs. 1-6 leads to the stiffness equations:

$$S_{L,x} = 2/(1/E_L - \nu_{L,T}/E_T) \quad (7)$$

$$S_{T,x} = 2/(1/E_T - \nu_{T,L}/E_L) \quad (8)$$

$$S_{ST,x} = -2/(\nu_{ST,L}/E_L + \nu_{ST,T}/E_T) \quad (9)$$

where, for example, $S_{L,x}$ is the measured stiffness in the long (principal) rolled direction due to stress in the loaded "x" direction. Finally, engineering constants reported in an earlier study [1] are substituted into Eqs. 7-9 for comparison with the current tests. Results shown in Table 3 are in satisfactory agreement except for an order of magnitude difference in the short-transverse stiffness. This may be due to a gage factor error.

Biaxial Failure

Based on results from the second and third specimens, failure strength is 533 MPa (77.32 ksi), which is 3.45 MPa (500 psi) less than the failure stress when the material is loaded only in the transverse (secondary) direction, and 31.0 MPa (4.50 ksi) lower than the failure stress predicted for a specimen loaded only in the long (primary) rolled direction.

TABLE *3. Comparison of Lockheed's Transformed Engineering Constants with Observed Stiffness*

Stiffness	Experiment		Lockheed	
	GPa	(10^3 ksi)	GPa	(10^3 ksi)
E_x	294.96	(42.78)	295.23	(42.82)
$S_{y,x}$	-3,061.96	(-444.10)	-3,753.5	(-544.40)
$S_{L,x}$	643.49	(93.33)	646.73	(93.80)
$S_{T,x}$	637.49	(92.46)	635.01	(92.10)
$S_{ST,x}$	1,989.55	(288.56)	18,084	(2,623.00)
$G_{L,T}$	137.14	(19.89)	136.86	(19.85)

Compressive State of Stress

Experimental and Numerical Studies

Knowledge of maximum in-plane compressive strengths, σ_1 and σ_2, is required for estimation of failure coefficients F_1, F_{11}, and F_{166} as well as F_2, F_{22}, and F_{266} (see References [3-5]). Numerical models were constructed prior to laboratory testing to aid in geometrical optimization of the experimental specimens, as suggested in reference [6]. Both two- and three-dimensional models of a simple compression specimen were generated (Figs. 7 and 8). The final design yielded a 38.1-mm x 12.7-mm (1.5-in. x 0.5-in.) experimental plate specimen (Fig. 9). Special fixtures were machined from A-2 tool steel, hardened to Rockwell C 50/55, and oriented to ensure that the specimens would not slip during loading (Fig. 10).

Eight hundred, eight-noded plate elements are used in a two-dimensional model of the structure with approximately 16,500 degrees-of-freedom. Only one-fourth of the actual structure is numerically modeled in order to capitalize on conditions of symmetry. Predictions at five integration points are requested in the through-thickness direction. Output at the top and bottom surfaces of the plate is compared with data from strain gages. A fringe plot of simulated axial displacements is shown in Fig. 11.

Symmetry conditions are also exploited for three-dimensional analysis. In this case, only one-eighth of the structure is modeled with four hundred, twenty-

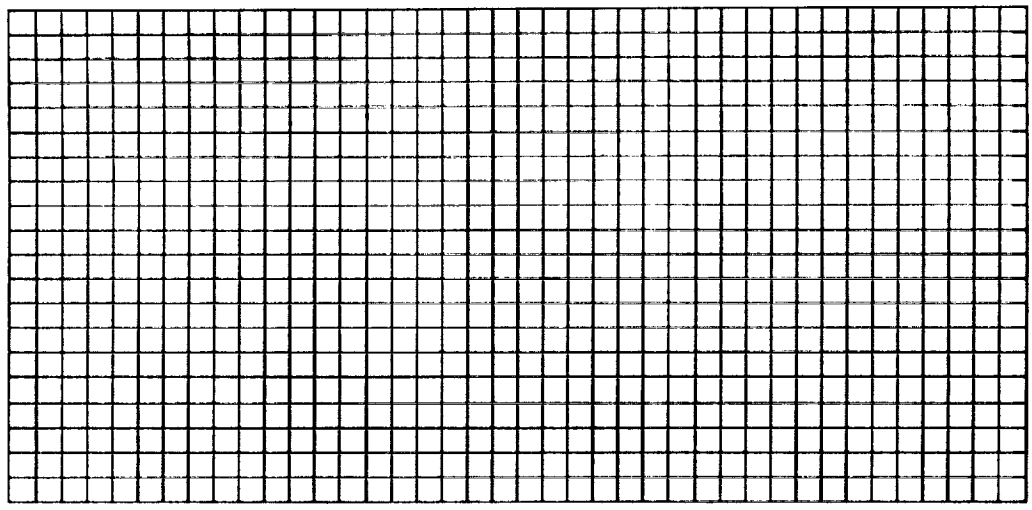

Figure *7 Two-dimensional In-Plane Compression Model Finite Element Mesh*

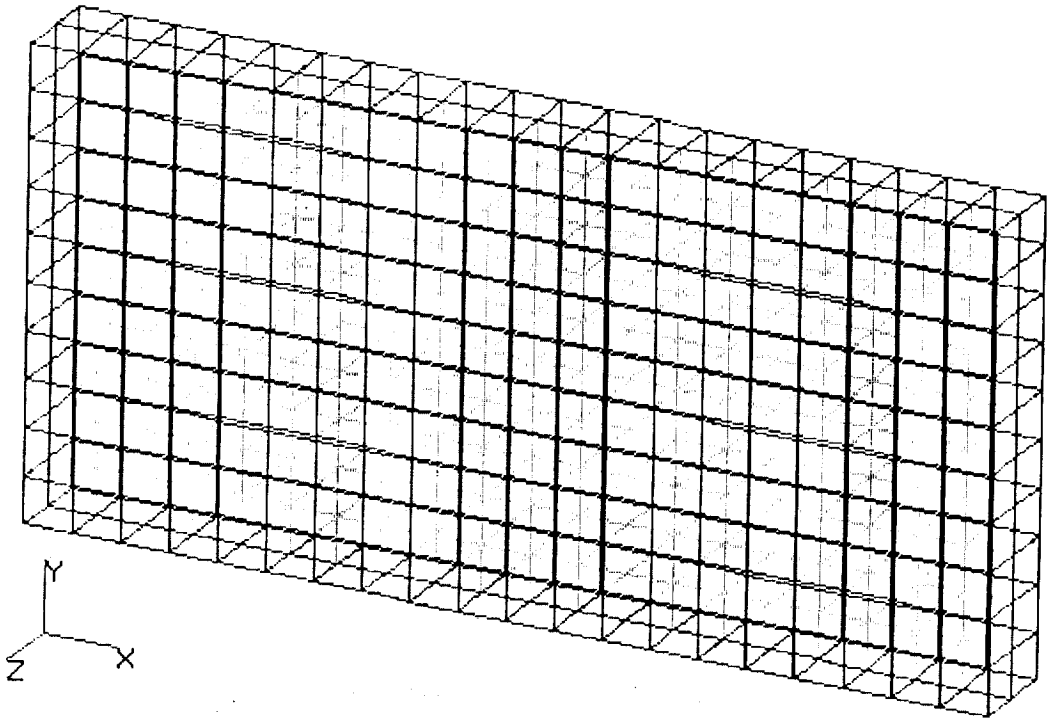

Figure *8 Three-Dimensional In-Plane Compression Model Finite Element Mesh*

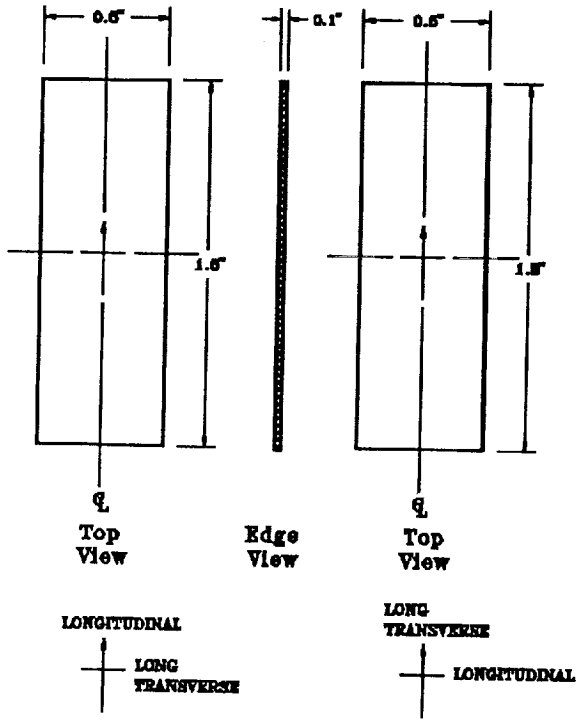

Figure *9 Compression Specimens*

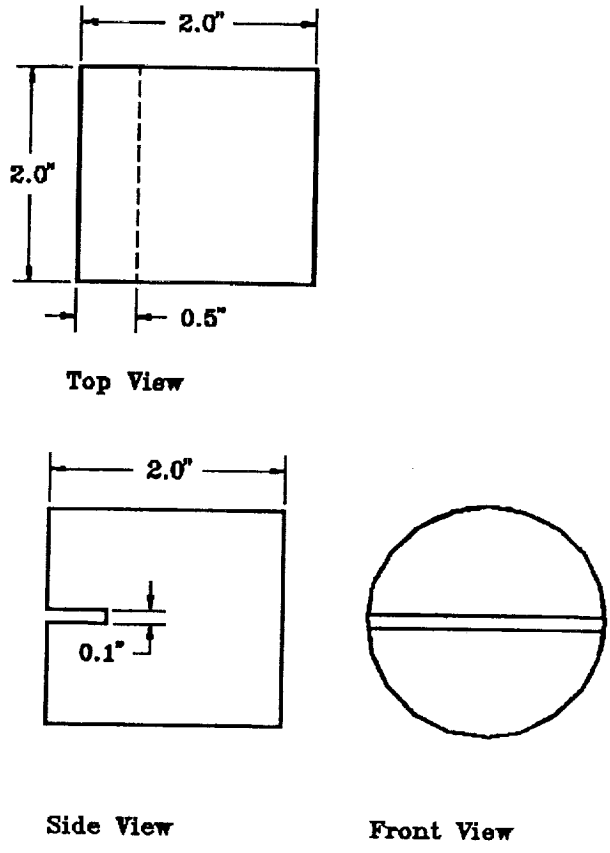

Figure *10 Compression Fixture*

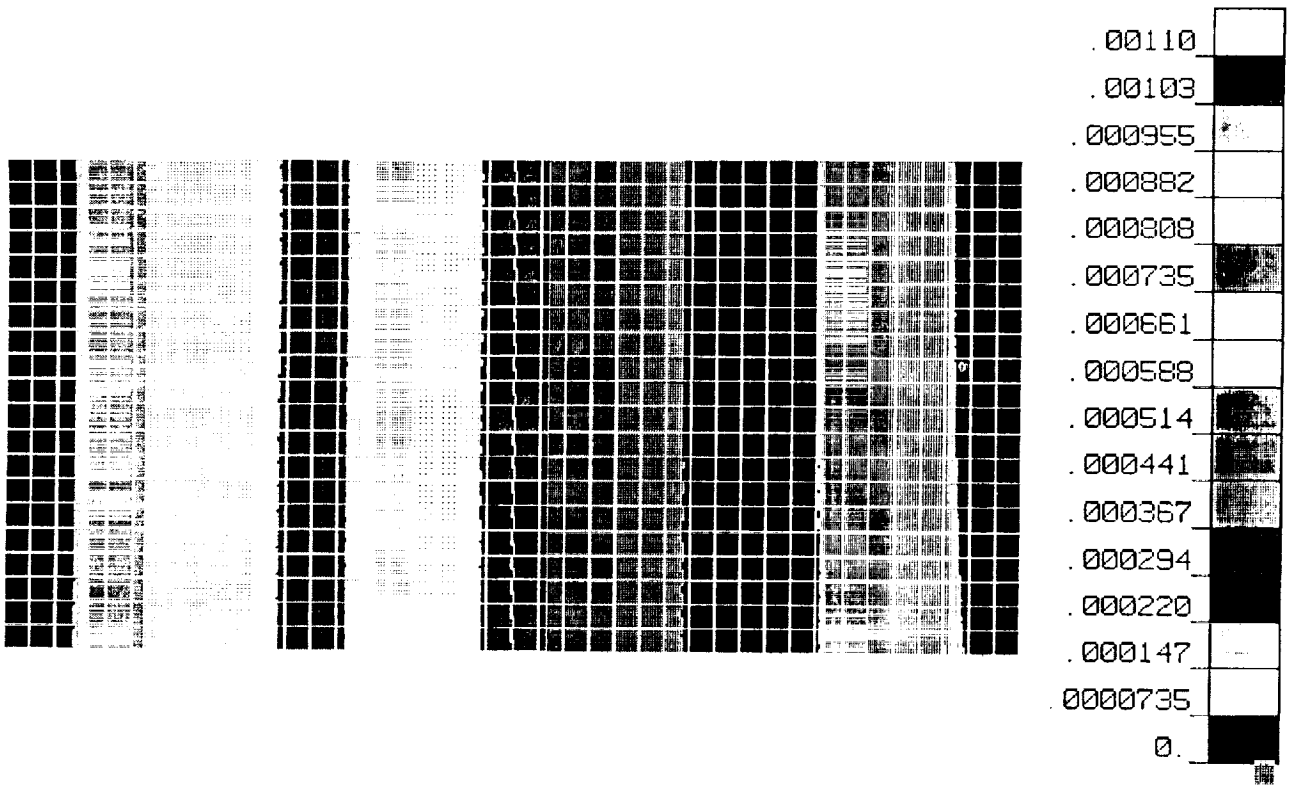

Figure *11 Axial Displacement Distribution for Two-Dimensional Compression FEA*

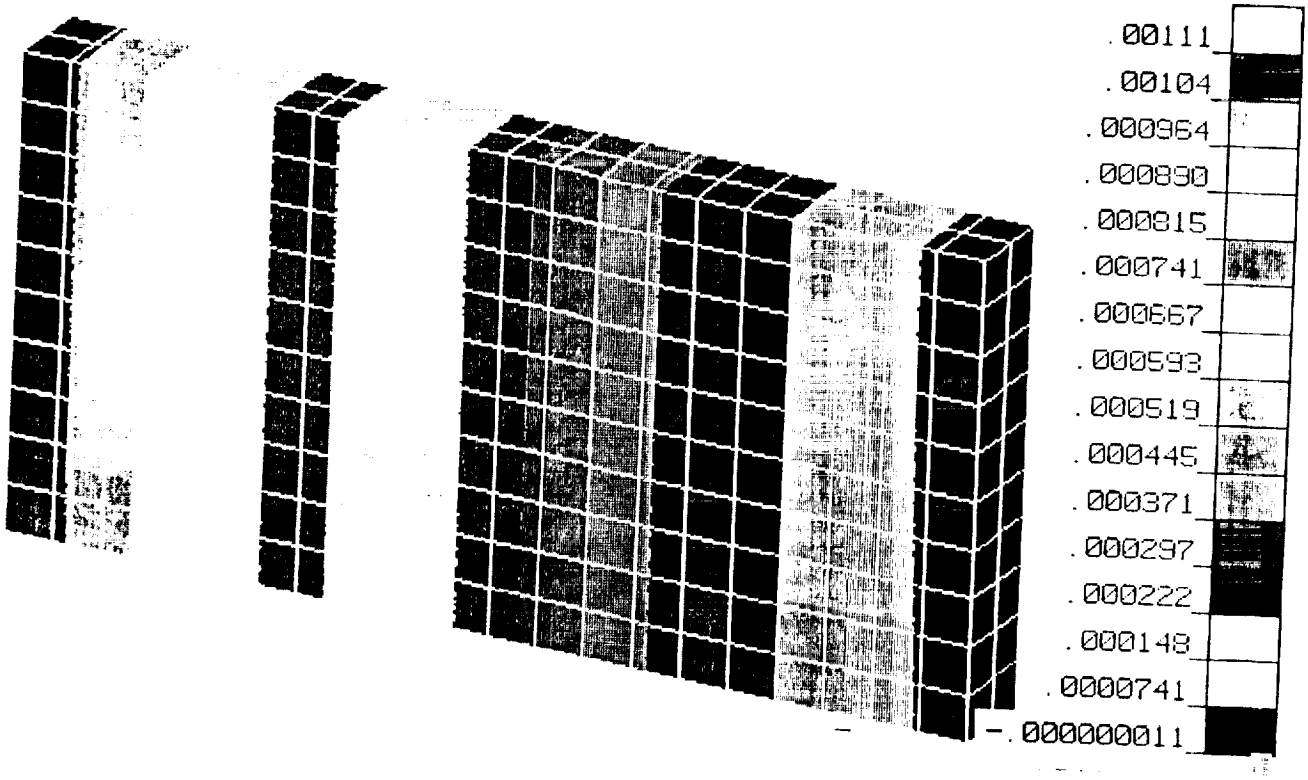

Figure *12 Axial Displacement Distribution for Three-Dimensional Compression FEA*

noded hexahedral elements. At the same time four elements are used to model the plate in the through-thickness direction. Results from the two- and three-dimensional analysis are in close agreement. Fringe patterns in Figs. 12 and 13 illustrate axial displacement and stresses reported by the three-dimensional model.

Compression testing was carried out on two specimens. One coupon had the longitudinal principal material axis oriented along the loading axis; the other had the long-transverse principal material axis coinciding with the direction of the load (Fig. 9). The specimens were loaded using a 44.5-kN (10-kip) capacity biaxial Material Testing Machine (MTS) (tension/compression-torsion) machine. In-plane strain was measured using bonded Micro-Measurement precision rosettes (CEA-06-062UR-350) that were placed on each side of the specimen directly opposite from each other. This was done to ensure symmetric distribution of the load. As a check, prior to actual testing the specimens were lightly loaded and the stress-strain curves of corresponding rosette strain gages were compared. Both specimens were loaded at a rate of 445 N/s (100 lb/sec).

Discussion of Test Results

Although the primary objective of this test is to obtain compressive strength coefficients for the longitudinal and long-transverse directions, the experiments also verify results obtained by other investigators, as well as serve to recalculate and compare the elastic moduli with results acquired from biaxial tests. Fig. 14 shows one of the specimens after failure. Stress-strain curves for specimens loaded with the principal axis of rolling that is parallel and perpendicular, respectively, to the load are plotted in Figs. 15 and 16. Strains plotted are for gages oriented in the direction of the load. Fig. 17 is similar to Figs. 15 and 16 but uses data collected from gages oriented 45° from the loading direction. The average modulus of elasticity is determined to be 3.00×10^5 MPa (43.8×10^6 psi). Table 4 summarizes the failure strength determined for each specimen.

TABLE *4. Failure Strength for Compression Specimens*

Specimen Number	Failure Stress	
	MPa	(ksi)
1	658.79	(95.55)
2	691.82	(100.34)

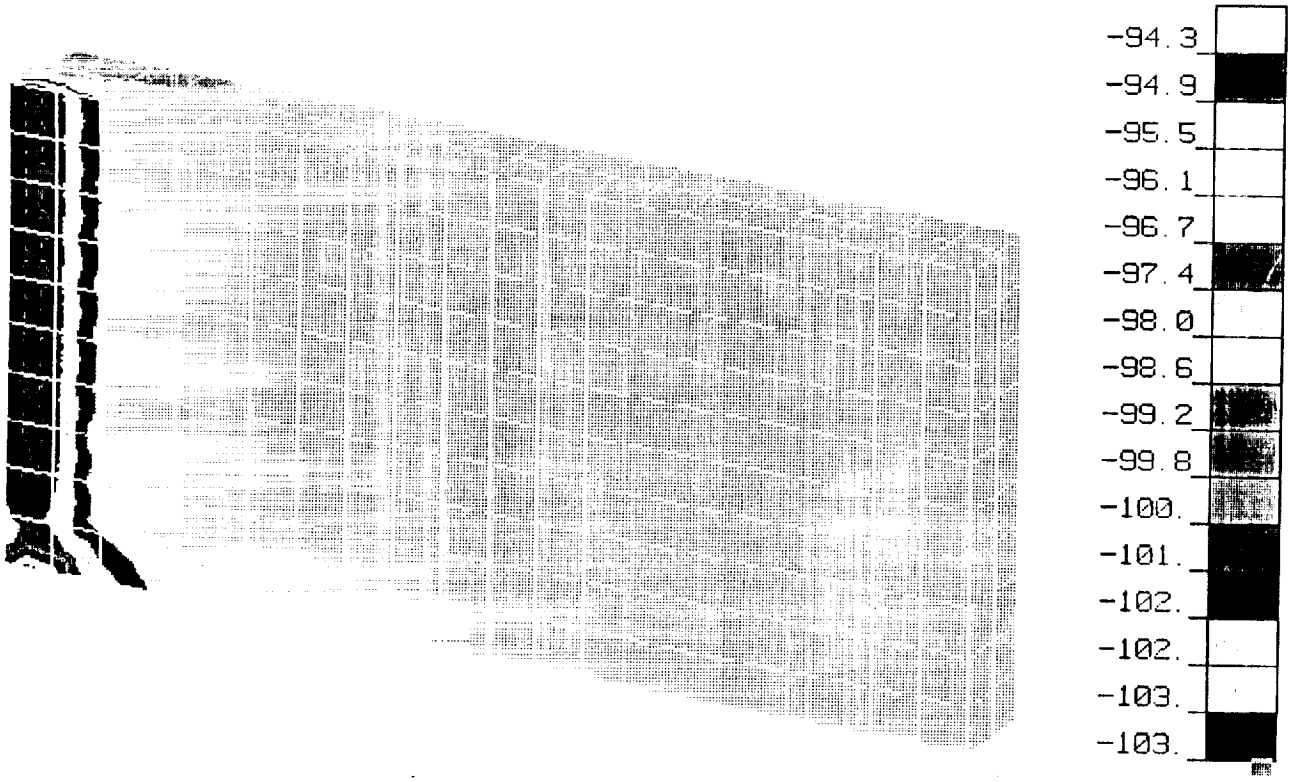

Figure *13 Axial Stress Distribution for Three-Dimensional Compression FEA*

Figure *14 Fractured Compression Specimen - Direction of Loading Aligned with Principal Material Axis*

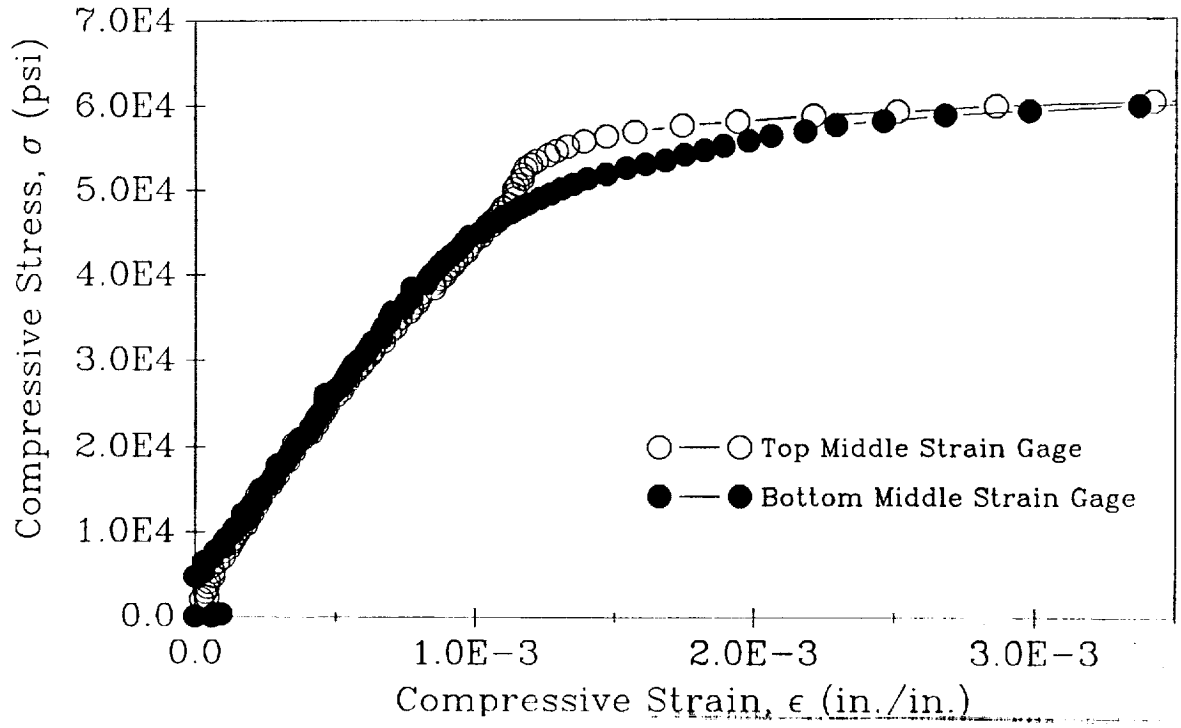

Figure *15 Stress vs. Strain in the Load Direction for Specimen with Principal Axis of Rolling Parallel to Load*

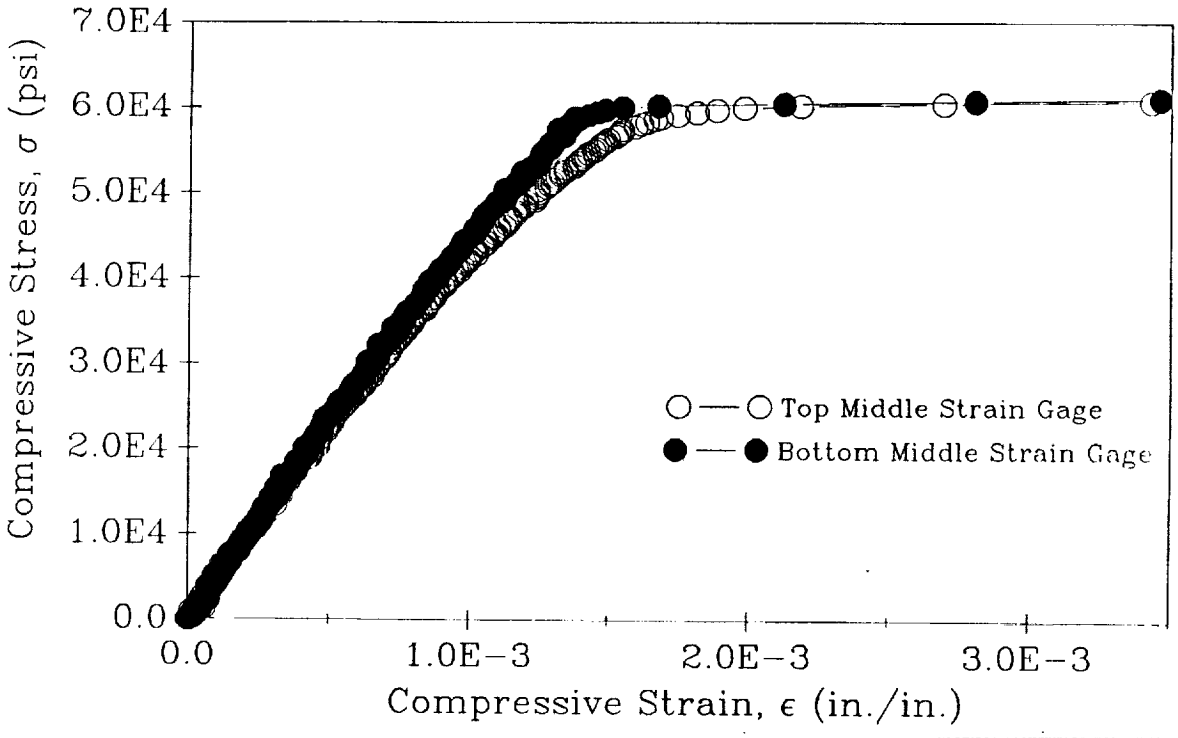

Figure *16 Stress vs. Strain in the Load Direction for Specimen with Principal Axis of Rolling Perpendicular to Load*

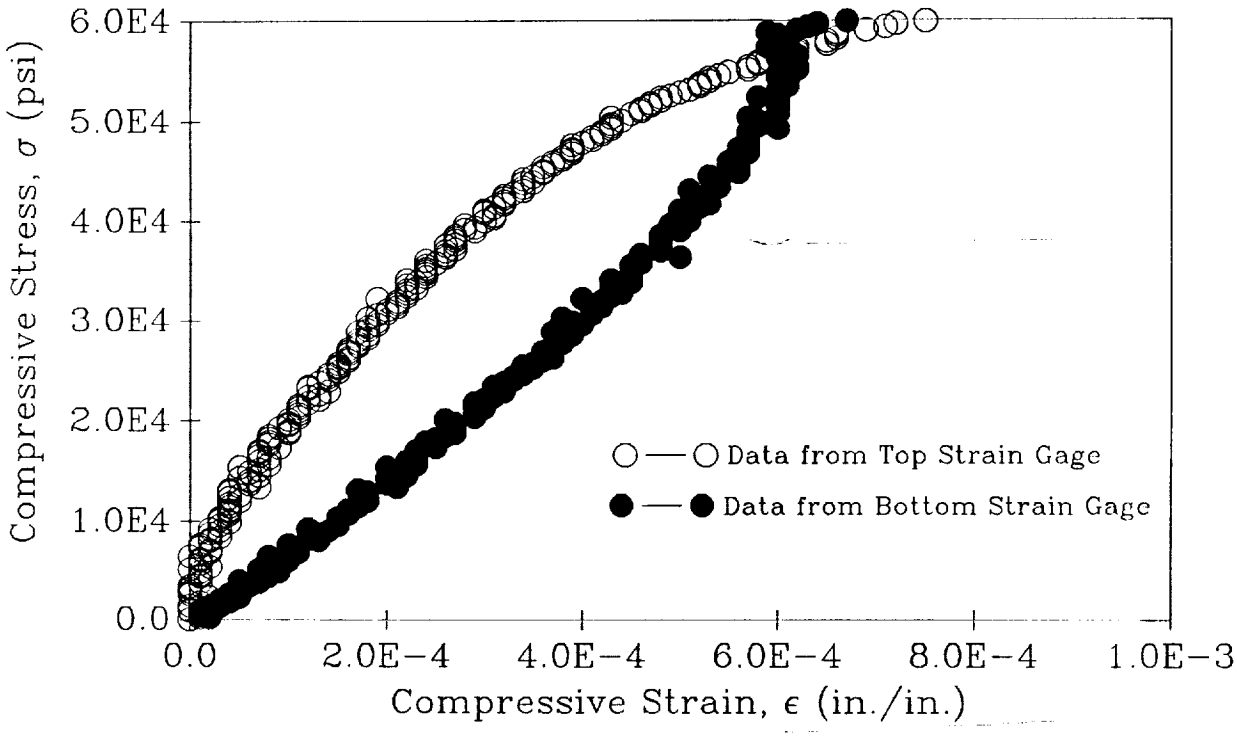

Figure *17 Stress vs. Strain at 45° from Load Direction for Specimen with Principal Axis of Rolling Perpendicular to Loading Direction*

Results obtained and the overall behavior of the compressive specimens are not unexpected. For both longitudinal and long-transverse specimens, the material fails catastrophically and exhibits properties distinctive of brittle material. Compressive strength, in both cases, appears to be approximately 20% higher than the tensile strength in the same direction, which is characteristic of brittle material. Elastic moduli, obtained from the stress-strain curves are slightly higher than moduli obtained from uniaxial tensile tests. Strain relations for orthotropic material undergoing uniform compressive load, σ_L^c, in the longitudinal direction follow from specialization of Eqs. 3-6:

$$\epsilon_L^c = \sigma_L^c / E_L \tag{10}$$

$$\epsilon_T^c = \nu_{T,L} (\sigma_L^c / E_L) \tag{11}$$

$$\epsilon_{ST}^c = \nu_{ST,L} (\sigma_L^c / E_L) \tag{12}$$

$$\gamma_{L,T}^c = \tau_{L,T}^c / G_{L,T} \tag{13}$$

Similarly, for a uniform compressive load, σ_T^c, in the long-transverse direction, Eqs. 3-6 yield:

$$\epsilon_T^c = \sigma_T^c / E_T \tag{14}$$

$$\epsilon_L^c = \nu_{L,T} (\sigma_T^c / E_T) \tag{15}$$

$$\epsilon_{ST}^c = \nu_{ST,T} (\sigma_T^c / E_T) \tag{16}$$

$$\gamma_{T,L}^c = \tau_{T,L}^c / G_{T,L} \tag{17}$$

Therefore, the strain tensor can be theoretically calculated and experimentally verified, provided the material is within the elastic range.

Conclusions

Experimental testing shows good correlation with numerical analysis and suggests that the numerical constitutive model is adequate. Principal failure coefficients F_1, F_2, F_{11}, and F_{22}, can be calculated from equations provided in Refs. [4] and [5], the in-plane tensile strength data (Lockheed [1]), and results of the compression experiment as follows:

$$F_i = (1 / X_i) - (1 / X_i')$$
$$F_{ii} = 1 / (X_i X_i') \tag{18}$$

where X_i and X_i' for i, j = 1, 2, and 3 are tensile and compressive strengths in the three principal directions of orthotropy. The resulting coefficients are:

$$
\begin{aligned}
F_1 &= 3.4153 \times 10^{-4}\ \text{MPa}^{-1} \quad (2.3548 \times 10^{-3}\ \text{ksi}^{-1}) \\
F_2 &= 3.2762 \times 10^{-4}\ \text{MPa}^{-1} \quad (2.2588 \times 10^{-3}\ \text{ksi}^{-1}) \\
F_{11} &= 2.8225 \times 10^{-6}\ \text{MPa}^{-2} \quad (1.3516 \times 10^{-4}\ \text{ksi}^{-2}) \\
F_{22} &= 2.5629 \times 10^{-6}\ \text{MPa}^{-2} \quad (1.2184 \times 10^{-4}\ \text{ksi}^{-2})
\end{aligned} \tag{19}
$$

Although beryllium is ductile when loaded under tension in its own plane, compressive loadings manifest very different behavior. Results obtained suggest that the material exhibits brittle properties for compressive in-plane loadings.

In-Plane Shear State of Stress

Experimental and Numerical Studies

Determination of the principal coefficient F_{66} [3], as well as interaction coefficients F_{166} and F_{266} [5], require knowledge of the in-plane shear strength, σ_6. Toward this end and prior to actual fabrication and physical testing, a numerical model is designed for simulation of a proposed in-plane shear test. Both two- and three-dimensional models are generated (Figs. 18 and 19). Material and geometrical nonlinearities are, once again, incorporated in the models. The actual specimen is a 101.6-mm x 25.4-mm (4-in. x 1-in.) coupon with two 45· slits located antisymetrically with respect to the x-x and y-y planes of symmetry.

As a preliminary test, titanium shear specimens were numerically modeled, fabricated, and loaded to failure. This material was chosen because of its availability and due to the fact that it has the same lattice microstructure, hexahedral-close-packed, as beryllium. Satisfactory correlation between numerical simulation and experimental data was determined for the shear strength of titanium. The mode of failure was pure shear.

The two-dimensional numerical model has two-thousand, eight-noded plate elements, which is equivalent to approximately 40,000 degrees-of-freedom. Five through-thickness points of integration are provided for each of the nine integration points per plate element. Numerical output is requested at each of the eight nodes for both the top and bottom surface of the elements (i.e. at integration points 1 and 5). A fringe plot showing axial displacements at the failure load of 3.89 kN (875 lb) is presented in Fig. 20.

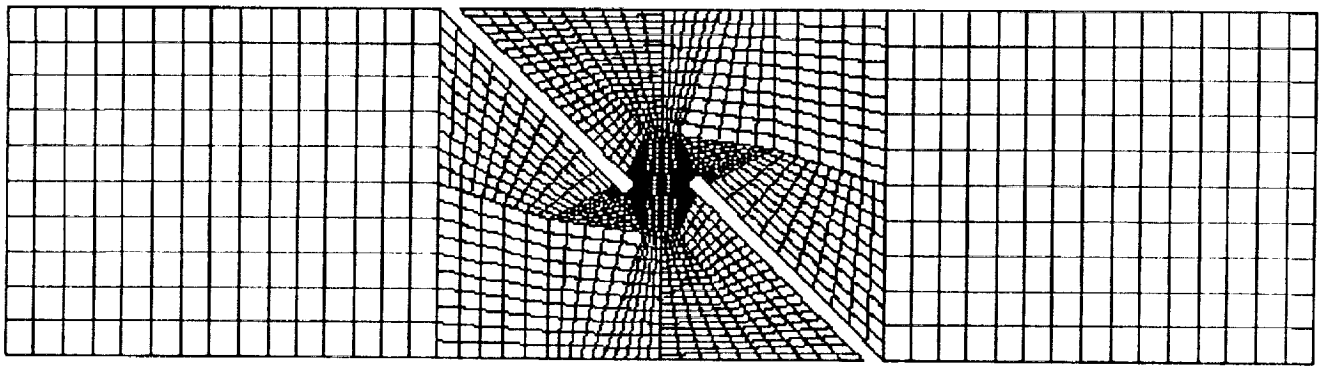

Figure *18 Two-Dimensional In-Plane Shear Model Finite Element Mesh*

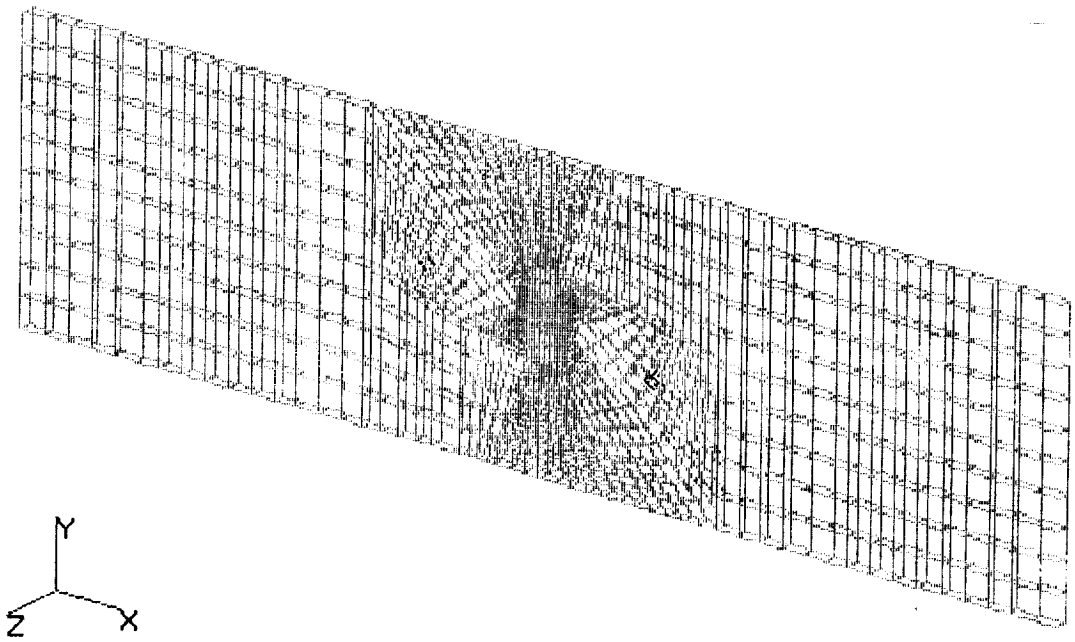

Figure *19 Three-Dimensional In-Plane Shear Model Finite Element Mesh*

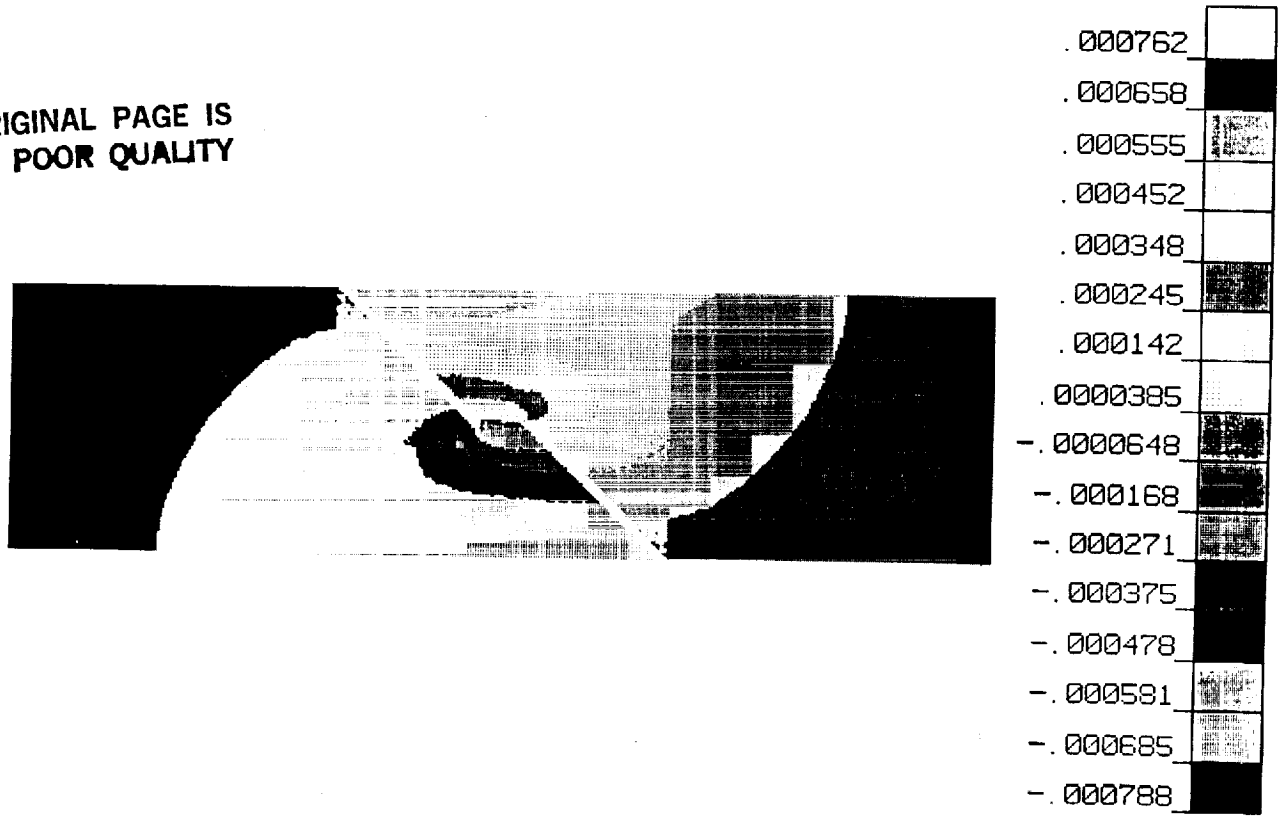

Figure *20 Fringe Plot of Axial Displacement for Two-Dimensional Shear*

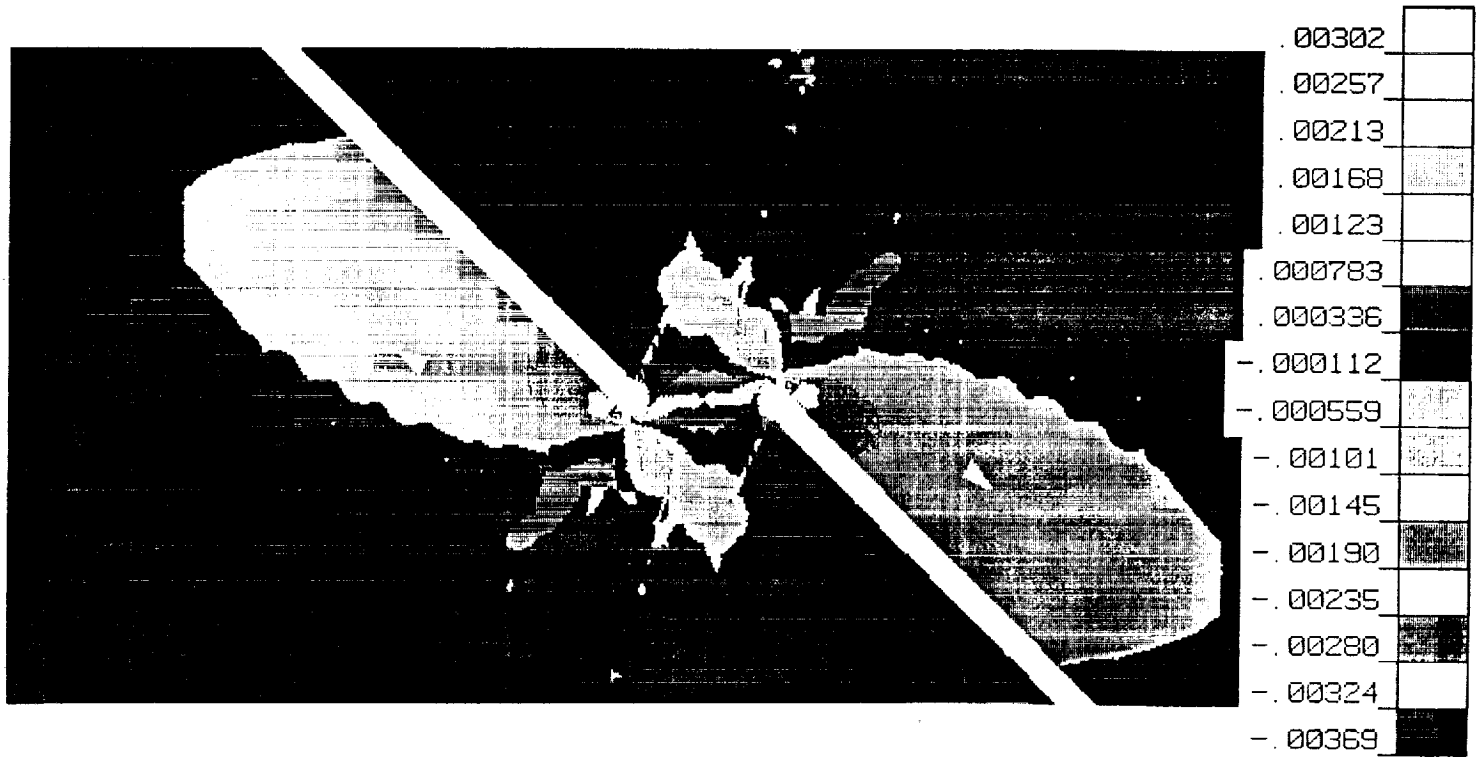

Figure *21 Fringe Plot of Shearing Strain for Three-Dimensional Shear*

For the three-dimensional model, 914 twenty-noded hexahedral elements are used. Due to symmetry of the geometry and load, only one-half of the actual structure is simulated. Two elements model the plate in the through-thickness direction. Fig. 21 shows a fringe plot of numerical output for in-plane shearing strains at failure.

Discussion of Test Results

Two experimental specimens, similar to the one shown in Fig. 22, are used to estimate the shearing strength of beryllium. Unlike titanium, a mixed mode of failure appears to dominate for beryllium. The material fails in a combined state of shear and axial tension. Thus, the experiment can not be regarded as a totally successful means for estimating shearing strength. However, via transformation of the stress tensor, a state of pure shear can be achieved on rotated differential elements (Fig. 23) that yields an average value of 344.74 MPa (50.0 ksi). This value of in-plane shearing strength appears to be satisfactory and is verified by another experiment recently conducted by NASA.

Conclusions

Experimental testing shows good correlation with numerical analysis. This suggests that the constitutive model utilized for numerical simulation is adequate for the type of analysis performed.

After careful examination of the failed surface, the mixed mode of failure, tension-shear, can be attributed partially to the fact that the through-thickness surfaces of the slits, especially around the center of the specimen, were heavily oxidized. Surface cracks may have formed prematurely and induced a mixed mode of failure.

Summary

Appendix B lists the in-plane shear and all other experiments required for the evaluation of polynomial coefficients for the cubic failure theory. Table 7 summarizes general experiments required for a continuum, while Table 8 shows a special subset of these experiments that provide coefficients necessary for thin plane failure prediction. Updated lists of all strength coefficients and their numerical values needed to establish Tsai-Wu [5] and the higher-order criterion [4] equations for cross-rolled beryllium sheet material are given in Tables 9 and 10.

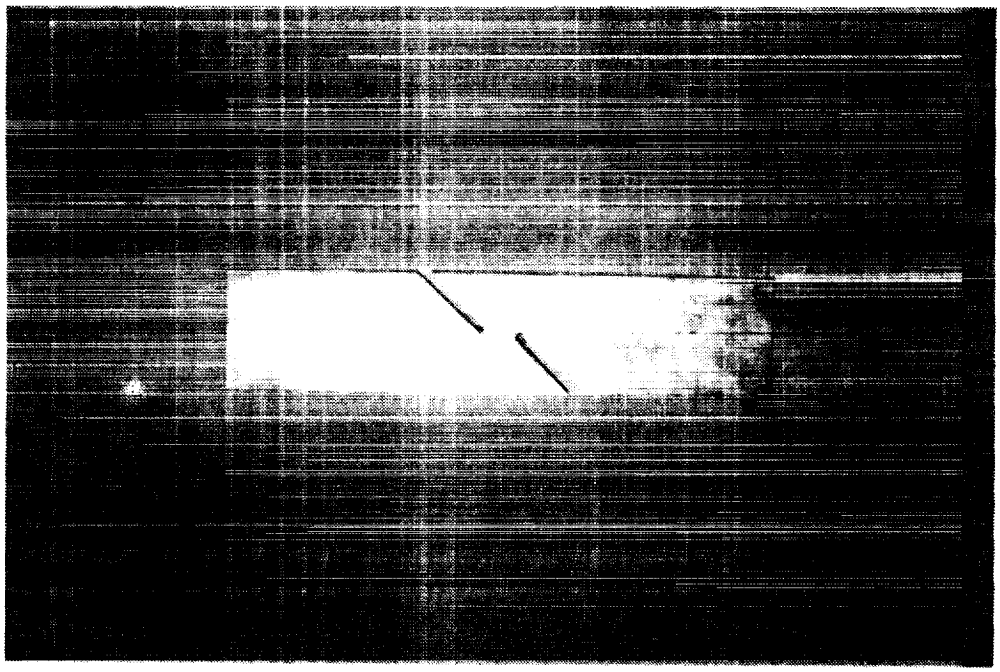

Figure *22 In-Plane Shear Specimen*

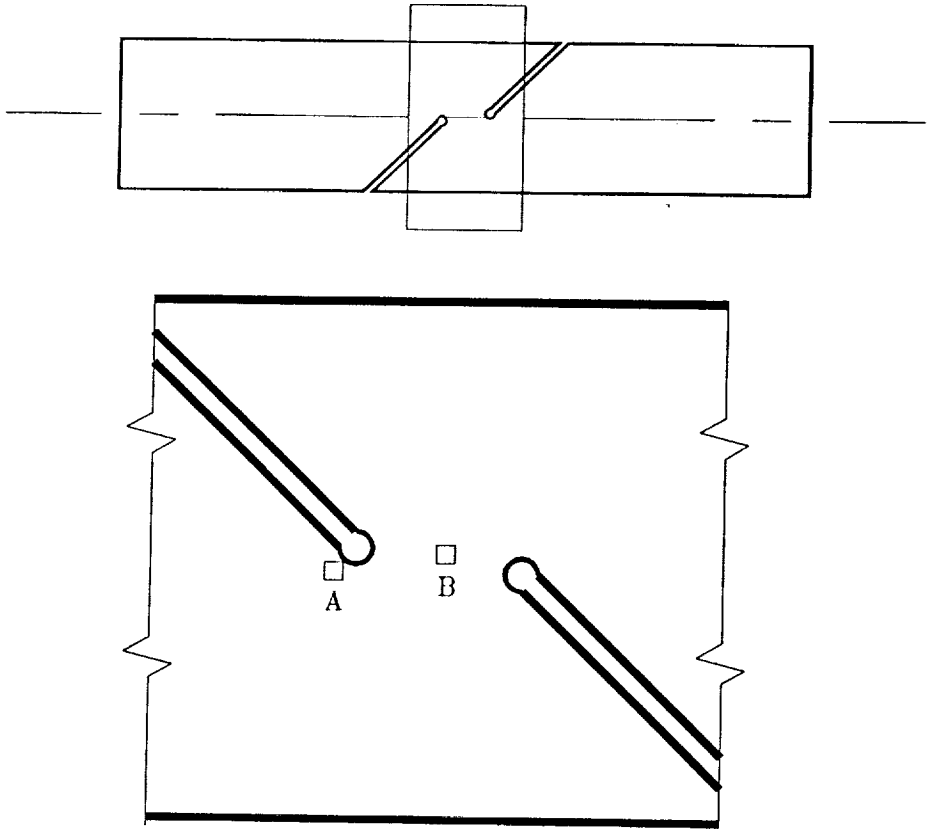

Figure *23 Location of Stress Transformation Elements*

CLAMPED PLATES WITH OUT-OF-PLANE POINT LOAD

Three clamped plates (numbered 2, 3, and 4 in Table 5) subjected to a central point load were tested. Primary purpose of these tests is to verify the failure criteria described earlier and to add to the existing beryllium data base of known material behavior. A hardened steel rod was used to impose the load. Clear spans of the tested plates varied from 50.8 mm x 50.8 mm (2 in. x 2 in.) to 101.6 mm x 101.6 mm (4 in. x 4 in.). Specimen 1 has not yet been tested. Specimen 4 has been loaded only to its initial failure point.

Experimental Procedure

Specimens 2, 3 and 4 were monitored with multiple TML gages, type FLE-1-350-11 (Figs. 24-26), and loaded to failure in an 87-kN (20-kip) MTS machine. Specimen dimensions shown are from support to support. To provide material to simulate a clamped-edge condition actual plate sizes are 50.8-mm (2.0-in.) longer in the transverse direction and 38.1-mm. (1.5-in.) longer in the longitudinal direction. Clamped edge conditions were achieved by a specially designed fixture (Fig. 26).

TABLE 5. *Dimensions of Square Clamped Plate Bending Specimens*

Specimen Number	Longitudinal Clear Span		Transverse Clear Span	
	mm	(in.)	mm	(in.)
1	25.4	(1.0)	25.4	(1.0)
2	50.8	(2.0)	50.8	(2.0)
3	75.1	(3.0)	75.1	(3.0)
4	100.2	(4.0)	100.2	(4.0)

Loading for each test was carried out by a hardened steel rod having a contact radius of 3.175 mm (0.125 in.). Rate of loading was approximately 8.2 N/s (1.85 lb/sec). All specimens were tested at a room temperature of approximately 22° C (72° F).

Results

The laboratory results show an intriguing tendency of cross-rolled beryllium to maintain strength after initial failure. The load versus deflection curve of specimen 3 (Fig. 27) shows a primary failure followed by an ultimate failure at

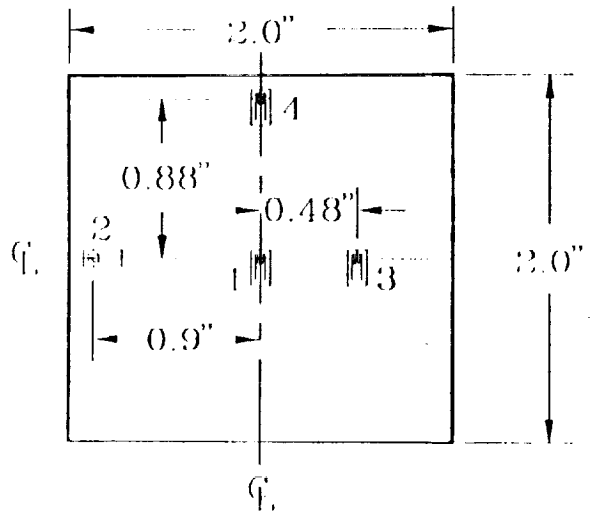

Figure *24 Strain Gage Location for Specimen 2*

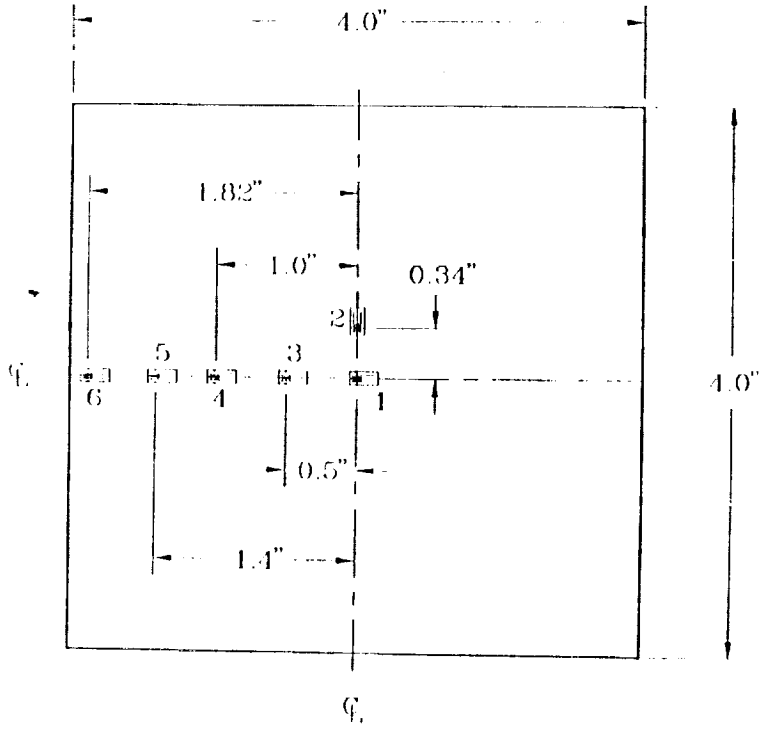

Figure *25 Strain Gage Location for Specimen 3*

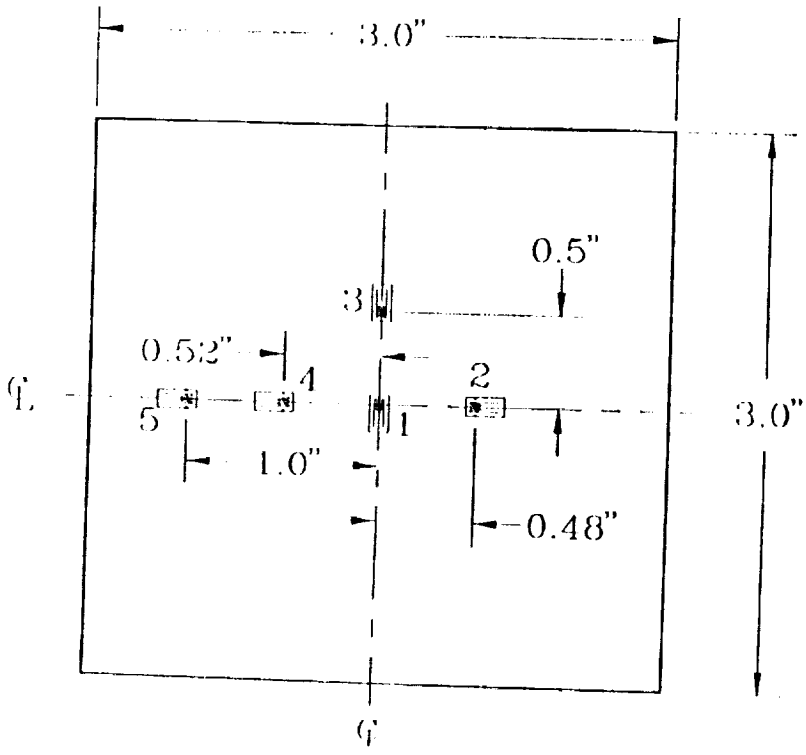

Figure *26 Strain Gage Location for Specimen 4*

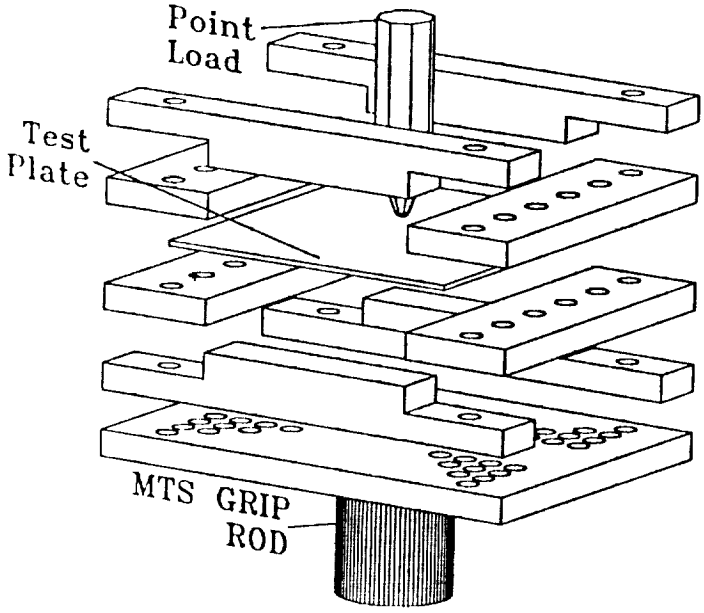

Figure *27 Clamped Plate Bending Test Fixture*

approximately 170% of the primary failure. Specimens 2 and 3 initially failed at 2.4 kN (530 lbs) and 2.2 kN (484 lbs), respectively. The impactor completely penetrated these plates at an ultimate strength of 4.2 kN (923 lbs) and 3.5 kN (769 lbs), respectively. Most strain gages display a linear response to the load before the initial failure, followed by a nonlinear relationship afterwards. An exception occurs for the gage located directly under the point of loading (Fig. 28). At this point of localized stress concentration, strain response becomes nonlinear after approximately 60% of the initial failure load.

A photograph of failed specimens 2 and 3 (Fig. 30) reveals a star-shaped pattern with a number of cracks radiating from the point of loading. Specimens 2 and 3 depict five- and four-point stars, respectively, within a circular area that has been punched out. Diameters of these circular areas are proportional to their plate dimensions. Also, close inspection of the specimens themselves reveals that delaminations in the middle surface of the plate may be seen along the edges of these circular openings.

Specimen 4 was loaded to its primary failure load, 2.1 kN (480 lb), followed by unloading. Careful visual examination showed no damage on the top surface (loading side) and four barely visible cracks radiating from the center of the bottom surface (Fig. 31). Depth of the cracks is unknown. Attempts will be made to determine these dimensions and extent of any delamination before the plate is loaded to ultimate strength.

Conclusions

Since specimens 1 and 4 have not been tested to ultimate failure and numerical modeling has not been completed, conclusions are pending for these specimens. After the entire series of plates have been tested, more definite conclusions can be reached for beryllium sheet material loaded out of its own plane.

Future Directions

Specimen 1 will be tested in the same fashion as specimen 4. The extent of damage and structural integrity will then be determined.

The test fixture was designed to accommodate a variety of length-to-width plate ratios. Table 6 lists the dimensions of a series of plates that are to be tested. Each has a different span length or length-to-width ratio. These plate specimens will be ordered and tested after experimentation on specimens 1 and 4 is complete. The variety of aspect ratios in this test matrix will provide important biaxial data for design of beryllium plate structures.

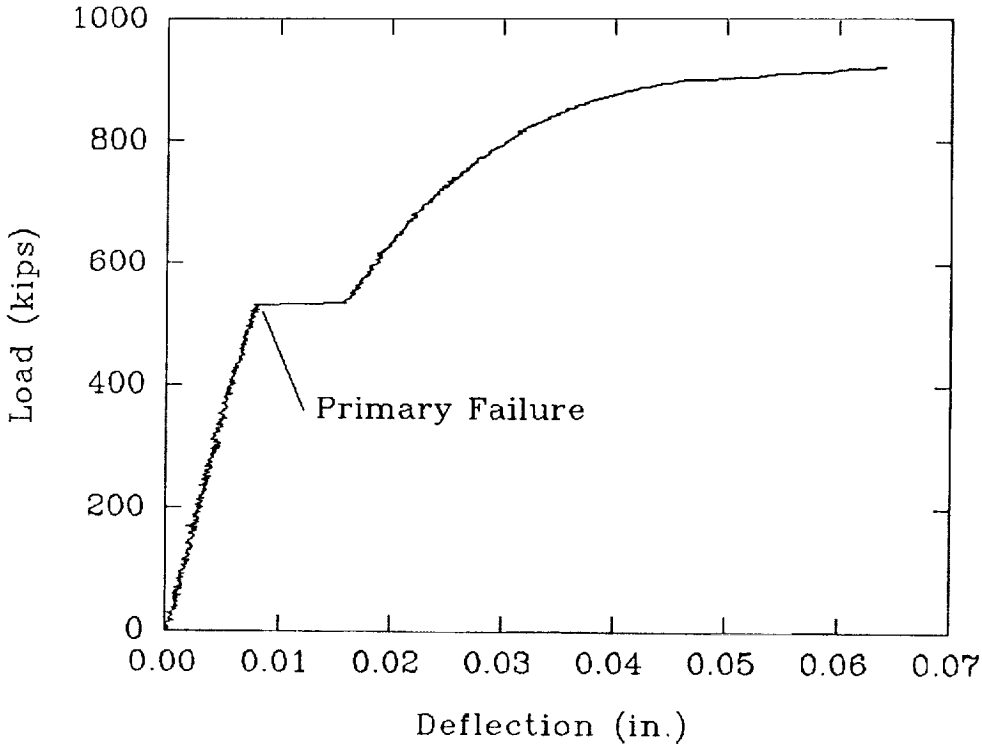

Figure *28 Load vs. Deflection for Specimen 3*

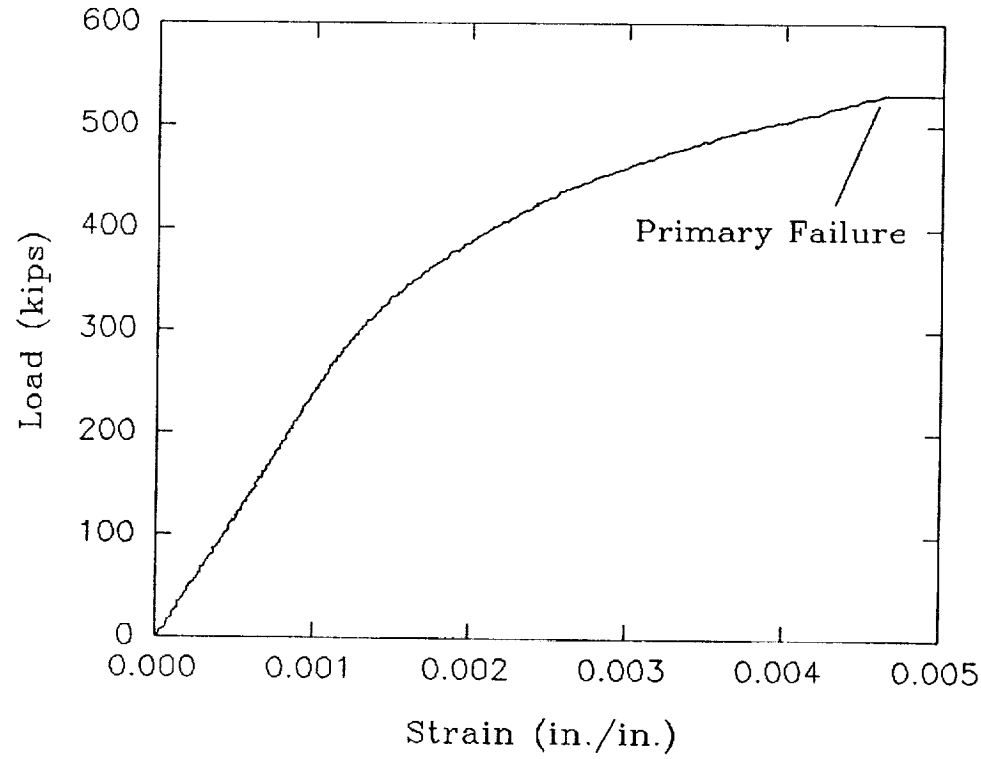

Figure *29 Load vs. Strain for Specimen 3*

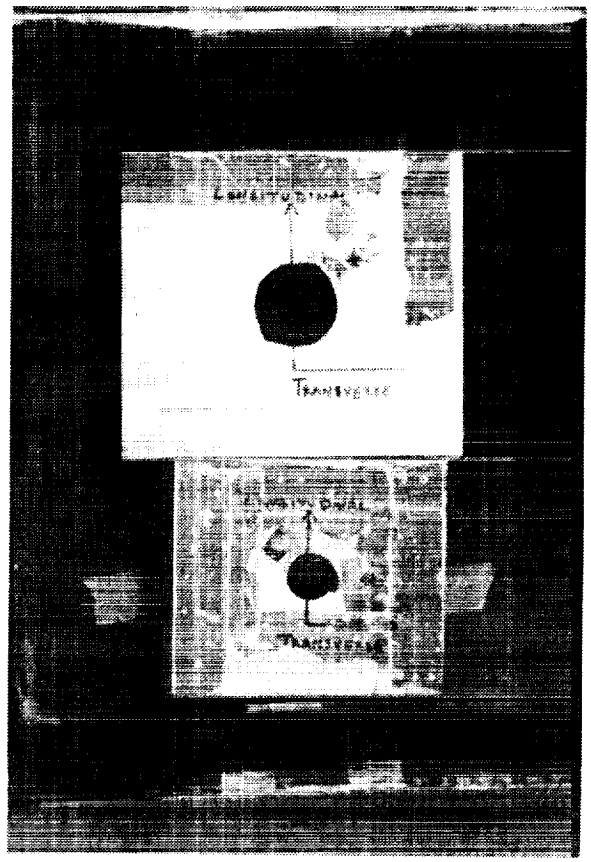

Figure *30 Failed Specimens 2 and 3*

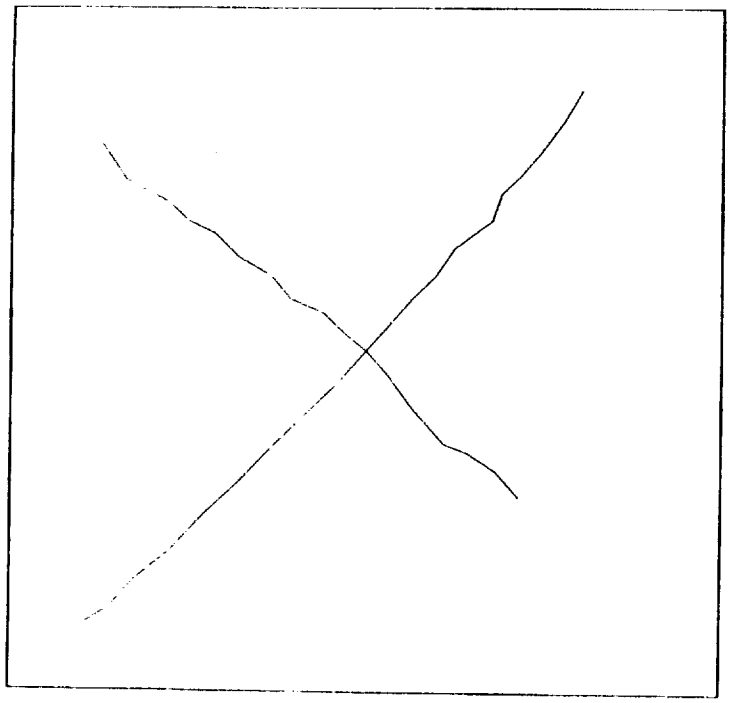

Figure *31 Crack Propagation Pattern for Specimen 4*

TABLE 6. *Nominal Dimensions of Clamped Plate Bending Specimens*

Longitudinal[a]		Transverse[a]		Number of
mm	(in.)	mm	(in.)	Specimens
25.4	(1.0)	50.8	(2.0)	1
25.4	(1.0)	75.1	(3.0)	1
25.4	(1.0)	100.2	(4.0)	1
50.8	(2.0)	25.4	(1.0)	1
50.8	(2.0)	75.1	(3.0)	1
50.8	(2.0)	100.2	(4.0)	1
75.1	(3.0)	25.4	(1.0)	1
75.1	(3.0)	50.8	(2.0)	1
75.1	(3.0)	100.2	(4.0)	1
100.2	(4.0)	25.4	(1.0)	1
100.2	(4.0)	50.8	(2.0)	1
100.2	(4.0)	75.1	(3.0)	1

[a]Actual specimen dimensions are 5.1-mm (2-in.) longer in one direction and 38.1 mm (1.5 in.) in the other.

Appendix A: Calculations

General transformation of stress tensors is as follows:

$$\sigma_{ij} = \alpha_{ki}\ \alpha_{lj}\ \sigma_{kl} \tag{20}$$

where α_{ki} and α_{li} are direction cosines for a second order tensor transformation.

In matrix form Eq. 20 becomes:

$$[\sigma_{MAT}] = [R]^T\ [\sigma_{LAX}]\ [R] \tag{21}$$

where [R] is a matrix of direction cosines relating the coordinate and material axes. For an in-plane biaxial test $[\sigma_{LAX}]$ and [R] are as follows:

$$[\sigma_{LAX}] = \begin{bmatrix} \sigma_x & 0 & 0 \\ 0 & 0 & 0 \\ 0 & 0 & 0 \end{bmatrix}; \quad [R] = \begin{bmatrix} 0.707 & 0.707 & 0 \\ -0.707 & 0.707 & 0 \\ 0 & 0 & 0 \end{bmatrix} \tag{22}$$

Substituting $[\sigma_{LAX}]$ and [R] in Eq. 21 the following material stress tensor is obtained:

$$[\sigma_{MAT}] = \begin{bmatrix} \frac{1}{2} & \frac{1}{2} & 0 \\ \frac{1}{2} & \frac{1}{2} & 0 \\ 0 & 0 & 1 \end{bmatrix} \sigma_x \tag{23}$$

Comparing σ_{MAT} and σ_{ij}, the following relations are derived:

$$\sigma_L = \sigma_T = \sigma_{L,T} = 0.5\ \sigma_x \tag{24}$$

A. Properties of Material Axes

Using the constitutive equations for orthotropic material the following relations are obtained [1]:

$$\epsilon_L = (\sigma_L/E_L) - \nu_{L,T}\,(\sigma_T/E_T) - \nu_{L,ST}\,(\sigma_{ST}/E_{ST}) \tag{25}$$

$$\epsilon_T = (\sigma_T/E_T) - \nu_{T,L}\,(\sigma_L/E_L) - \nu_{T,ST}\,(\sigma_{ST}/E_{ST}) \tag{26}$$

$$\epsilon_{ST} = (\sigma_{ST}/E_{ST}) - \nu_{ST,L}\,(\sigma_L/E_L) - \nu_{ST,T}\,(\sigma_T/E_T) \tag{27}$$

$$\gamma_{L,T} = \tau_{L,T}/G_{L,T} \tag{28}$$

By substituting Eq. 24 into Eqs. 25-28, the following stress-strain relations are obtained:

$$\epsilon_L = 0.5\,[\sigma_L\,(1/E_L - \nu_{L,T}/E_T)] \quad (29)$$
$$\epsilon_T = 0.5\,[\sigma_L\,(1/E_T - \nu_{T,L}/E_L)] \quad (30)$$
$$\epsilon_{ST} = -0.5\,[\sigma_L\,(\nu_{ST,L}/E_L + \nu_{ST,T}/E_T)] \quad (31)$$
$$\gamma_{L,T} = 0.5\,[\sigma_L/G_{L,T}] \quad (32)$$

Moreover, stiffness coefficients are obtained as follows [1]:

$$S_{L,x} = \sigma_x / \epsilon_L = 2/(1/E_L - \nu_{L,T}/E_T) \quad (33)$$
$$S_{T,x} = \sigma_x / \epsilon_T = 2/(1/E_T - \nu_{T,L}/E_L) \quad (34)$$
$$S_{ST,x} = \sigma_x / \epsilon_{ST} = -2/(\nu_{ST,L}/E_L + \nu_{ST,T}/E_T) \quad (35)$$

By substituting strength values and Poisson's ratios obtained from the biaxial test and an earlier report [1], the following stiffness matrix coefficients are obtained:

$$S_{L,x} = 646.73 \text{ GPa } (93.8 \times 10^6 \text{ psi})$$
$$S_{T,x} = 635.01 \text{ GPa } (92.1 \times 10^6 \text{ psi}) \quad (36)$$
$$S_{ST,x} = 17.93 \text{ GPa } (2.6 \times 10^6 \text{ psi})$$

B. Properties of Loading Axes

The strain tensor can be transformed from material to loading axes as follows:

$$[\epsilon_{MAT}] = [R]\ [\epsilon_{LAX}]\ [R]^T \quad (37)$$

since, $[R]^T = [R]^{-1}$. For the case of biaxial loading the relations obtained from such a transformation are:

$$\epsilon_x = 0.5\,(\epsilon_L + \epsilon_T + 2\,\epsilon_{L,T}) \quad (38)$$
$$\epsilon_y = 0.5\,(\epsilon_L + \epsilon_T - 2\,\epsilon_{L,T}) \quad (39)$$

where ϵ_L, ϵ_T, and ϵ_{ST}, are estimated from Eqs. 23-25. Therefore, the modulus of elasticity, E_x, and the stiffness coefficient, $S_{y,x}$, for the loading axes are estimated as follows:

$$E_x = \sigma_y / \epsilon_x = 295.23 \text{ GPa } (42.82 \times 10^6 \text{ psi}) \quad (40)$$
$$S_{y,x} = \sigma_x / \epsilon_y = -3{,}753.51 \text{ GPa } (544.4 \times 10^6 \text{ psi}) \quad (41)$$

Appendix B: Strength Parameters

Table 7. *Experiments Required for Evaluation of Coefficients*

Experiment	Axis	Coefficients
Uniaxial:		
Tension and }		F_1, F_2, F_3
Compression }	X, Y, Z	F_{11}, F_{22}, F_{33}
Pure Shear:		
Positive }		F_4, F_5, F_6
or Negative }	X, Y, Z	F_{44}, F_{55}, F_{66}
Biaxial:		
Tension-Tension or }	X-Y	F_{12}, F_{112}, F_{122}
Compression-Compression }	X-Z	F_{13}, F_{113}, F_{133}
or, Tension-Compression }	Y-Z	F_{23}, F_{223}, F_{322}
Combined:		
Tension or Compression }	X-Y	F_{166}, F_{266}
and }	X-Z	F_{144}, F_{344}
Shear }	Y-Z	F_{255}, F_{355}

Table 8. *Experiments Required for Evaluation of Coefficients for Plates*

Experiment	Axis	Coefficients
Uniaxial:		
Tension and }		F_1, F_2, F_3
Compression }	X, Y, Z	F_{11}, F_{22}, F_{33}
Pure Shear:		
Positive }		F_4, F_5, F_6
or Negative }	X, Y, Z	F_{44}, F_{55}, F_{66}
Biaxial and Shear:		
Tension-Tension or }	X-Y	$F_{12}, F_{112}, F_{122}, F_{166}, F_{266}$
Compression-Compression }	X-Z	$F_{23}, F_{223}, F_{322}, F_{244}, F_{344}$
or Tension-Compression }	Y-Z	$F_{13}, F_{113}, F_{133}, F_{155}, F_{355}$
with in-plane shear }		

TABLE *9. Failure Strength Coefficients for Cross-Rolled Beryllium Sheets Using the Tsai-Wu Model*

Strength Coefficient	Numerical Value	
F_1	3.54×10^{-4} MPa^{-1}	(2.44×10^{-3} ksi^{-1})
F_2	4.17×10^{-4} MPa^{-1}	(2.77×10^{-3} ksi^{-1})
F_3	8.70×10^{-4} MPa^{-1}	(6.00×10^{-3} ksi^{-1})
F_{11}	2.84×10^{-6} MPa^{-2}	(1.35×10^{-4} ksi^{-2})
F_{22}	2.67×10^{-6} MPa^{-2}	(1.27×10^{-4} ksi^{-2})
F_{33}	2.91×10^{-6} MPa^{-2}	(1.38×10^{-4} ksi^{-2})
F_{44}	3.72×10^{-6} MPa^{-2}	(1.77×10^{-4} ksi^{-2})
F_{55}	3.45×10^{-6} MPa^{-2}	(1.64×10^{-4} ksi^{-2})
F_{66}	1.09×10^{-5} MPa^{-2}	(5.17×10^{-4} ksi^{-2})
F_{12}	-2.56×10^{-6} MPa^{-2}	(-1.22×10^{-4} ksi^{-2})

Note: F_{13} and F_{23} are not yet available.

TABLE *10. Failure Strength Coefficients for Cross-Rolled Beryllium Sheets Using the New Proposed Criterion*

Strength Coefficient	Numerical Value	
F_1	3.54×10^{-4} MPa^{-1}	(2.44×10^{-3} ksi^{-1})
F_2	4.17×10^{-4} MPa^{-1}	(2.77×10^{-3} ksi^{-1})
F_3	8.70×10^{-4} MPa^{-1}	(6.00×10^{-3} ksi^{-1})
F_{11}	2.84×10^{-6} MPa^{-2}	(1.35×10^{-4} ksi^{-2})
F_{22}	2.67×10^{-6} MPa^{-2}	(1.27×10^{-4} ksi^{-2})
F_{33}	2.91×10^{-6} MPa^{-2}	(1.38×10^{-4} ksi^{-2})
F_{44}	3.72×10^{-6} MPa^{-2}	(1.77×10^{-4} ksi^{-2})
F_{55}	3.45×10^{-6} MPa^{-2}	(1.64×10^{-4} ksi^{-2})
F_{66}	1.09×10^{-5} MPa^{-2}	(5.17×10^{-4} ksi^{-2})
F_{12}	-1.29×10^{-6} MPa^{-2}	(-6.11×10^{-5} ksi^{-2})
F_{13}	-1.65×10^{-5} MPa^{-2}	(-7.82×10^{-4} ksi^{-2})
F_{112}	-6.90×10^{-10} MPa^{-3}	(-2.26×10^{-7} ksi^{-3})
F_{122}	-2.18×10^{-10} MPa^{-3}	(-7.14×10^{-8} ksi^{-3})
F_{166}	-1.14×10^{-10} MPa^{-3}	(-3.74×10^{-7} ksi^{-3})
F_{266}	-1.14×10^{-10} MPa^{-3}	(-3.74×10^{-7} ksi^{-3})
F_{113}	-5.82×10^{-7} MPa^{-3}	(-1.91×10^{-4} ksi^{-3})
F_{133}	9.31×10^{-8} MPa^{-3}	(3.05×10^{-5} ksi^{-3})
F_{144}	5.59×10^{-7} MPa^{-3}	(1.83×10^{-4} ksi^{-3})
F_{344}	-9.89×10^{-8} MPa^{-3}	(-3.24×10^{-5} ksi^{-3})

Note: F_{23}, F_{223}, F_{233}, F_{244}, F_{155}, F_{255}, F_{355}, and F_{366} are not yet available.

Appendix C: Notation

σ_x	=	stress parallel to the direction of the load
σ_L	=	stress in the long material direction
σ_T	=	stress in the transverse material direction
σ_{ST}	=	stress in the short transverse material direction
$[\sigma_{MAT}]$	=	material axis stress tensor
$[\sigma_{LAX}]$	=	load axis stress tensor
$[\epsilon_{MAT}]$	=	material axis strain tensor
$[\epsilon_{LAX}]$	=	load axis strain tensor
ϵ_L	=	strain in the long material direction
ϵ_T	=	strain in the transverse material direction
ϵ_{ST}	=	strain in the short transverse material direction
γ_{LT}	=	shear strain in the plane of the material
E_x	=	Young's modulus for load axis
E_L	=	elastic modulus for long material direction
E_T	=	elastic modulus for transverse material direction
E_{ST}	=	elastic modulus for short transverse material direction
$G_{L,T}$	=	in-plane shear modulus
$\nu_{y,x}$	=	in-plane Poisson's ratio
$\nu_{ST,x}$	=	through-thickness Poisson's ratio
$S_{y,x}$	=	measured stiffness in "y" direction due to stress in the "x" direction
$S_{L,x}$	=	measured stiffness in long material direction due to stress in the "x" direction
$S_{T,x}$	=	measured stiffness in transverse material direction due to stress in the "x" direction
$S_{ST,x}$	=	measured stiffness in short transverse material direction due to stress in the "x" direction
α_{ki}, α_{lj}	=	direction cosines for transformation of stress tensor

Appendix D: References

1. Fenn, R.W., Jr., Cooks, D.D., Kinder, W.C., and Lempiere, B.M., "Test Methods for Mechanical Properties of Anisotropic Materials (Beryllium Sheet)," *Technical Report AFML-TR-67-212*, Lockheed Missiles and Space Company, October, 1967.

2. Hill, R., *The Mathematical Theory of Plasticity*, Oxford, The Clarendon Press, 1950.

3. Tsai, S.W., Wu, E.M., "The Brittle Strength of Material," *J. Composites and Materials*, Vol. 1, pp. 200-206, 1967.

4. Priddy, T.G., "A Fracture Theory for Brittle Anisotropic Materials," *J. Engineering Materials and Technology*, pp. 91-96, April, 1974.

5. Roschke, P.R., Papados, P.P., Mascoro, E., "Failure Prediction of Thin Beryllium Sheets Used in Spacecraft Structures," *Annual Report*, NASA Grant Number: NAG 9-280, May, 1990.

6. Wu, E.M., Scheublein, J.K., "Laminate Strength - A Direct Procedure," *Compos. Mater.: Testing and Design (Third Conference)*, ASTM STP 546, 1974.